International Journal of Microwave and Wireless Technologies

cambridge.org/mrf

Dual band circularly polarized partially reflecting surface-loaded dielectric resonator-based MIMO antenna for mm-wave 5G applications

Pawan Kumar Shukla[1], Sikandar[2], Vijay Shanker Tripathi[1] and Anand Sharma[1]

[1]Department of Electronics and Communication Engineering, Motilal Nehru National Institute of Technology Allahabad, Prayagraj, India and [2]Department of Electronics Engineering, Rajkiya Engineering College, Sonbhadra, India

Research Paper

Cite this article: Shukla PK, Sikandar, Tripathi VS, Sharma A (2024) Dual band circularly polarized partially reflecting surface-loaded dielectric resonator-based MIMO antenna for mm-wave 5G applications. *International Journal of Microwave and Wireless Technologies* **16**(7), 1198–1207. https://doi.org/10.1017/S1759078724000163

Received: 28 September 2023
Revised: 4 January 2024
Accepted: 5 January 2024

Keywords:
circular polarization; dielectric resonator antenna; MIMO antenna; mm-wave

Corresponding author: Anand Sharma;
Email: anandsharma@mnnit.ac.in

Abstract

A two-port ceramic-based antenna loaded with partially reflecting surface (PRS) is structured and explored. Fan-shaped slot is utilized to create circularly polarized wave in both frequency ranges. Dual frequency ranges are due to hybrid mode creation inside the ceramic material, i.e. $HEM_{11\delta}$ and $HEM_{12\delta}$ modes. PRS is used to change the phase gradient, which in turn tilts the radiation beam ($\pm 35^{\circ}$) obtained from different port in opposite direction. This concept is useful to reduce the envelop correlation coefficient using far-field. Experimental verification confirms that the designed antenna works from 26.1 to 27.5 GHz and 31.7 to 33.6 GHz along with less than 3-dB axial ratio from 26.5 to 27.1 GHz and 31.9 to 33.1 GHz respectively. Orthogonal placement of ports introduces the concept of polarization diversity and decreases the coupling between ports by an amount of −25 dB. Good gain value (up to 7.0 dBi) and better value of diversity performance make the designed radiator applicable for 5 G millimeter-wave uses.

Introduction

In the modern domain of mobile communication, there is wide necessity of large data rate without enhancing the transmitted power. For fulfilling this requirement, two techniques are very famous in literature: (i) use of multiple input, multiple output (MIMO) communication system in order to improve the signal-to-noise ratio [1] and (ii) shifting of communication toward millimeter (mm)-wave/sub mm-wave frequency ranges [2]. Different types of antennas are available to fulfill the above requirement such as microstrip antenna or its array. However, these radiators suffer from high radiation losses at mm-wave frequency due to the presence of metallic and surface wave losses [3]. Dielectric resonator–based radiators remove the difficulties of metallic antennas because these are free from metallic and surface wave losses [4].

In literature, some articles are available in the area of mm-wave MIMO dielectric resonator antenna (DRA). Zhang et al. [5] designed a dual-port dielectric-based MIMO antenna, which works from 27.25 GHz to 28.59 GHz. Metallic strips are utilized on the top of the rectangular ceramic for further reducing the mutual coupling level up to −12 dB. Pan et al. [6] proposed a new technique to improve the isolation level between two-port ceramic antenna using the vias. This antenna design works from 25 to 27 GHz with an isolation level more than 40 dB. Murthy [7] used the concept of metallic strip over the ceramic to improve the isolation among the four ports. This radiator works from 26.6 GHz to 29.57 GHz with the isolation level around 17 dB. Hasan et al. [8] structured a dual-port ceramic-based radiator and used hybrid isolator between the ports to enhance the isolation. It works from 58.8 GHz to 63.6 GHz with an isolation level around 40 dB. Alanazi et al. [9] designed an aperture-coupled rectangular ceramic at mm-wave frequency. It supports dual frequency ranges (i.e. 27.9–28.8 GHz and 37.89–38.02 GHz) with isolation around 27 dB by placing the radiators on opposite side of the substrate. Kumar et al. [10] proposed a dual-port CDRA at mm-wave frequency range. With the assistance of plus-shaped aperture, it creates circularly polarized (CP) waves in between the working frequency range (i.e. 25.5–27.79 GHz). Sharma et al. [11] designed a dual-port ceramic-based filtenna, which works from 27.9 to 28.5 GHz. Antiparallel placing of ports improves the isolation level to more than 30 dB. From the aforementioned literature, it is clear that still the work is required of improving the diversity performance in far-field region. Varshney et al. [12–14] proposed different shapes of ceramic to create

CP waves and improve the impedance bandwidth in DR-based MIMO antennas such as, semicircular ceramic, Z-shaped ceramic, and epsilon-shaped ceramic. Varshney et al. [15] designed an aperture-coupled rectangular ceramic to create wide-band characteristics by combining the three different operating modes.

In this article, a designing of dual-port dual band CP ceramic-based radiator is discussed. Partially reflecting surface (PRS) is also suspended over the antenna in order to tilts the beam by an amount of $\pm 30^{\circ}$. Due to this, the value of ECC (by far-field) is reduced and diversity performance becomes good in far-field region. Fan-shaped aperture creates the CP waves in dual frequency ranges, i.e. 26.5–27.1 GHz and 31.9–33.1 GHz, respectively. For better understanding, the given article is segmented in various sections: (i) geometrical layout, (ii) antenna analysis, (iii) experimental outcome, and (iv) conclusion.

Geometrical layout of the designed radiator

Figure 1 presents the structural layout of the designed antenna with different views. The substrate utilized to structure the dual-port antenna and PRS is Rogers RT 5880 substrate($\varepsilon_r = 2.2; \tan\delta = 0.0009$). The thickness of the substrate

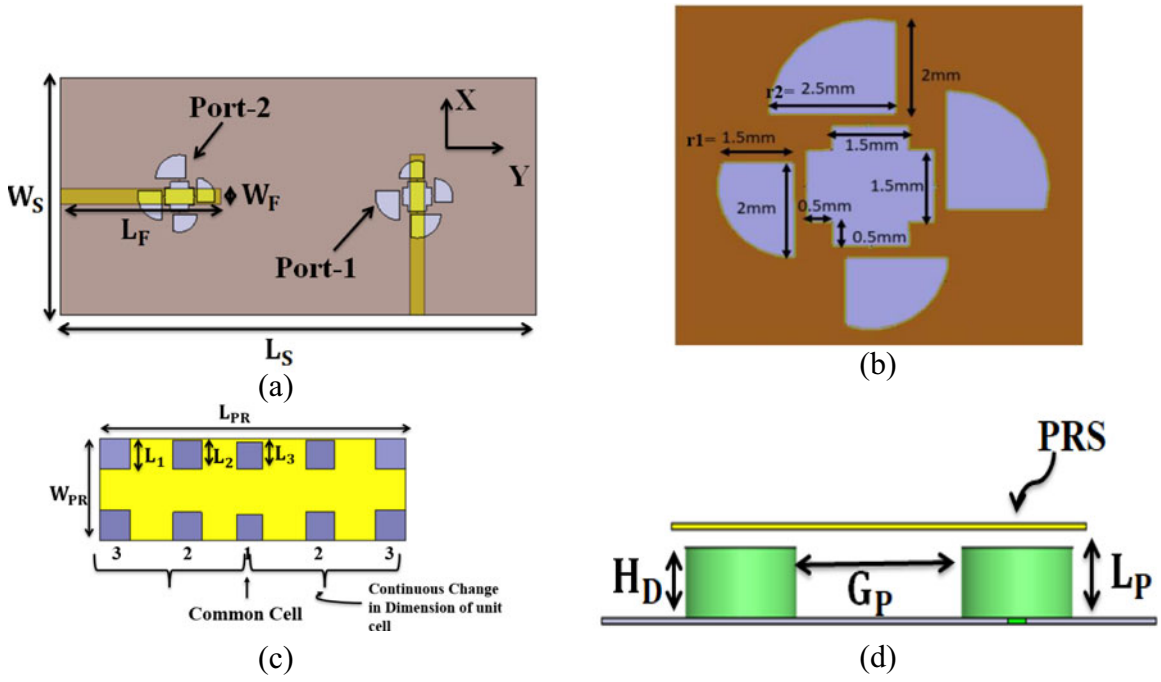

Figure 1. Geometrical layout of the designed radiator: (a) feeding structure, (b) expanded view of aperture, (c) partial reflecting surface, (d) side view of antenna.

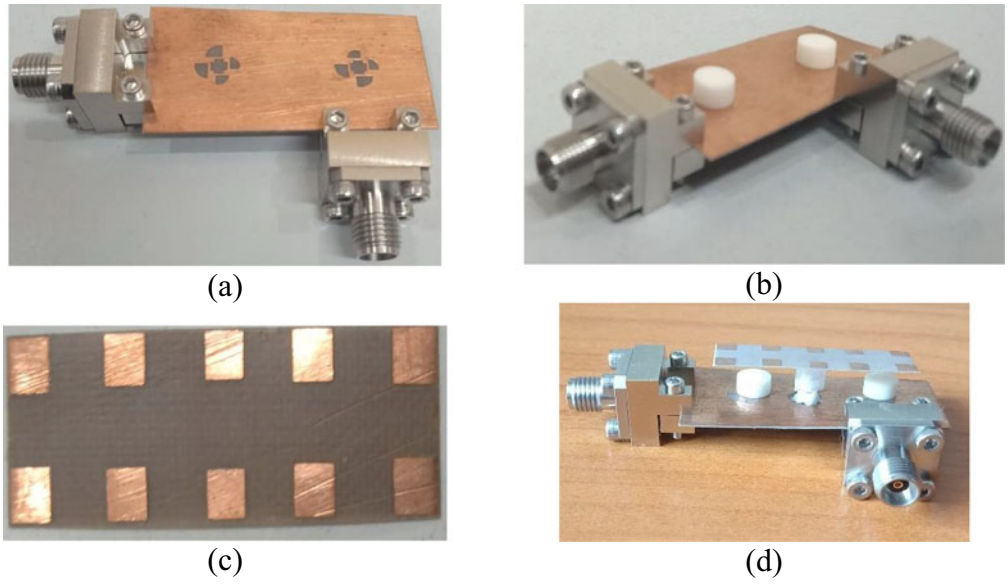

Figure 2. Pictures of fabricated antenna: (a) designed aperture, (b) dual-port ceramic antenna, (c) partially reflecting surface, (d) 3D view of the proposed antenna.

https://doi.org/10.1017/S1759078724000163 Published online by Cambridge University Press

Table 1. Optimized dimension of the designed mm-wave dual-port antenna

Symbol	Dimension (mm)	Symbol	Dimension (mm)
W_S	20.0	L_F	13.5
L_S	40.0	L_2	1.8
W_F	1.3	L_3	1.6
L_1	2.0	L_P	5.0
H_D	3.0	G_P	5.0
W_{PR}	10.0	L_{PR}	30.0

is 0.254 mm. Fan-shaped aperture has been etched from the substrate to excite the ceramic material. The ceramic material used as substrate is alumina having permittivity of 9.8 and loss tangent of 0.002. The optimized diameter (D) of cylindrical ceramic is taken as 8.0 mm. Table 1 lists the optimized dimension of various parameters of the proposed radiator. Figure 2 shows the pictures of fabricated radiator.

Analysis of the designed radiator

In this section, the detailed analysis of the designed radiator has been carried out using high-frequency structure simulator electromagnetic simulator. The analysis of the proposed antenna starts with single-port structure. Figure 3 shows the reflection coefficient variation of the designed antenna in the presence and absence of ceramic material. From Fig. 3, it is observed that the complete frequency band is due to the cylindrical ceramic material. Spectrum shown in Fig. 3 has two significant resonant peaks at 26.2 GHz and 32.1 GHz, respectively. In order to find the accountability of these resonances, Fig. 4 shows the E-field variation on cylindrical ceramic at 26.2 GHz and 32.1 GHz, respectively. From Fig. 4, it is confirmed that the resonant peaks at 26.2 GHz and 32.1 GHz

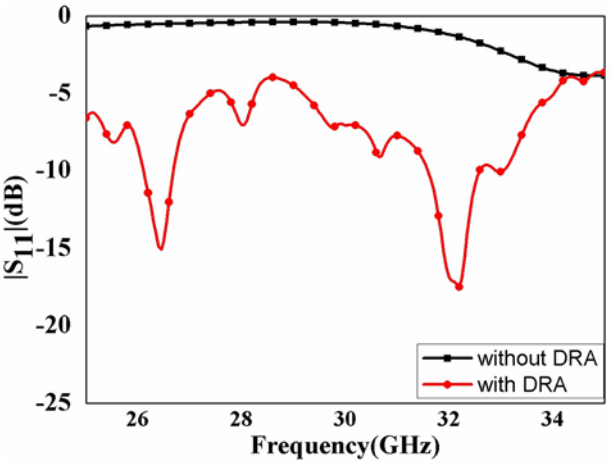

Figure 3. $|S_{11}|$ variation in the presence and absence of DRA for single-port antenna.

are due to $HEM_{11\delta}$ and $HEM_{12\delta}$ modes, respectively [16]. These resonant peaks can also be calculated as follows [17]:

$$f_{r,HEM_{11\delta}} = \frac{6.321c}{\pi D\sqrt{\varepsilon_{r,eff}+2}}\left[0.27+0.36\left(\frac{D}{4H_D}\right)+0.02\left(\frac{D}{4H_D}\right)^2\right] \quad (1)$$

In eqn. (1), D and H_D denote the diameter and height of the alumina ceramic, respectively. From eqn. (1), the resonant frequency is found to be 25.95 GHz. In literature, no empirical formula is available to calculate the resonant frequency of $HEM_{12\delta}$ mode. However, it can be predicted on the basis aspect ratio of cylindrical ceramic by using the following formulation [18]:

$$f_{r,HEM_{12\delta}} \geq 1.25 \times f_{r,HEM_{11\delta}} \quad (2)$$

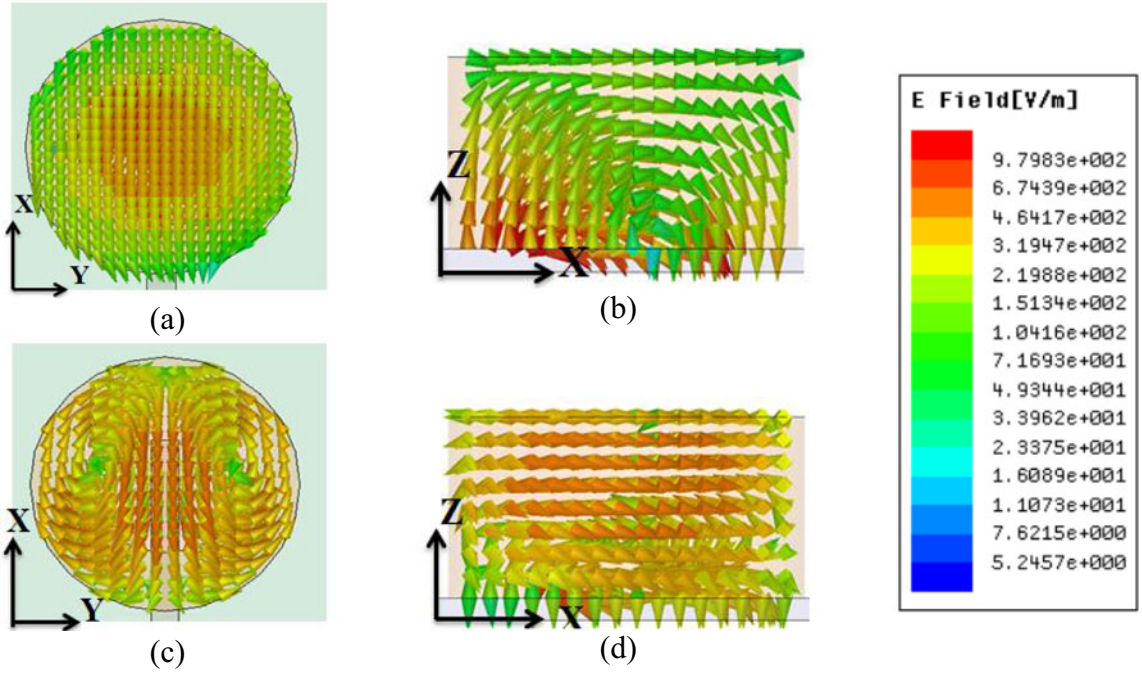

Figure 4. E-field on cylindrical ceramic: (a) top view at 26.2 GHz, (b) side view at 26.2 GHz, (c) top view at 32.1 GHz, (d) side view at 32.1 GHz.

https://doi.org/10.1017/S1759078724000163 Published online by Cambridge University Press

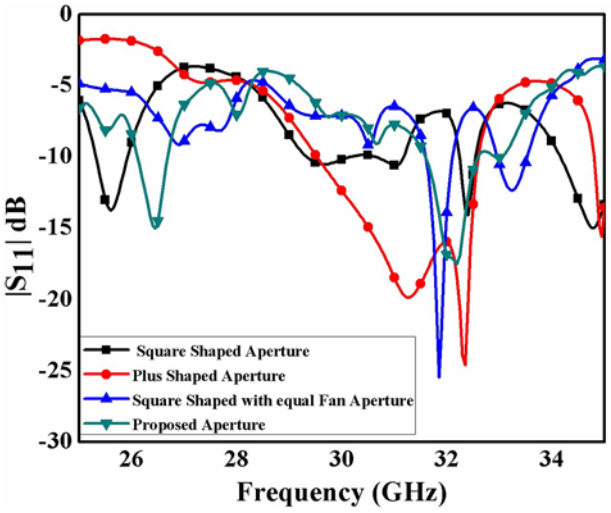

Figure 5. $|S_{11}|$ variation with different changes in the aperture of single-port antenna.

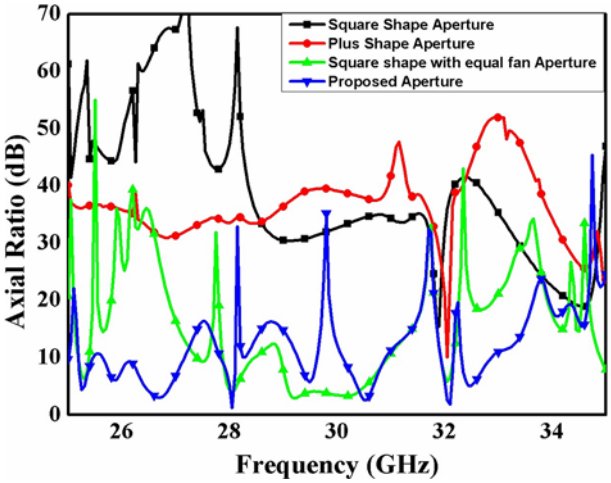

Figure 6. Axial ratio variation with different changes in the aperture of single-port antenna.

From eqn. (2), the resonant frequency of $HEM_{12\delta}$ mode is $\geq$32.43 GHz, which is closer to the simulated outcome.

Figure 5 shows the reflection coefficient ($|S_{11}|$) curve with various modifications in the shape of the aperture. Four different shapes are taken into the account: (i) square-shaped aperture, (ii) plus-shaped aperture, (iii) equal fan along with plus-shaped aperture, and (iv) unequal fan-shaped with plus-shaped aperture (proposed). From Fig. 5, it can be perceived that both the frequency bands are obtained with all shapes of aperture. However, only the impedance matching of each band is changing with aperture shape. The best reflection coefficient is achieved in the proposed case. One more thing is observed from Fig. 5 that square-/plus-shaped aperture is capable of creating both the hybrid modes, i.e. $HEM_{11\delta}$ and $HEM_{12\delta}$. Aperture acts as a magnetic dipole, so it will be able to generate $HEM_{11\delta}$. It is a very well known fact that $HEM_{12\delta}$ mode is the orthogonal mode of $HEM_{11\delta}$. Square-shaped aperture excites the *x*-polarized and *y*-polarized waves with equal strength [19]. Due to which, $HEM_{12\delta}$ mode is also produced by square-/plus-shaped aperture at 32.1 GHz. Figure 6 shows the axial ratio variation with the aforementioned changes in the shape of aperture. It can be perceived from Fig. 6 that in case of asymmetrical fan-shaped aperture-loaded ceramic, the CP waves are obtained in both the operating bands. In the proposed aperture, fan blades are aligned orthogonally. These blades are able to create the orthogonal modes with equal amplitude. Now, change in the size of blades (make it asymmetrical) creates the path delay between the field line. This will result in the phase difference. Parametric analysis has been done to create the phase difference of 90°, which is shown in Fig. 7. It can be observed from Fig. 7(a) and (b) that as the fan blade size becomes nonuniform, the axial ratio moves toward the 3-dB down. In this wave, the necessary condition to create CP waves has been fulfilled by the proposed antenna [20].

After that, single-port antenna is converted into the dual port. There are two possibilities with dual-port antenna: (i) parallel orientation and (ii) perpendicular orientation. Figure 8 shows the reflection coefficient comparison of single-port and dual-port (with parallel and perpendicular orientation) antennas. From Fig. 8, it is confirmed that the reflection coefficient curve is approximately same in all three cases. Figure 9 shows the mutual coupling curve variation in parallel and perpendicular orientation of dual-port antenna. From Fig. 9, it is confirmed that mutual

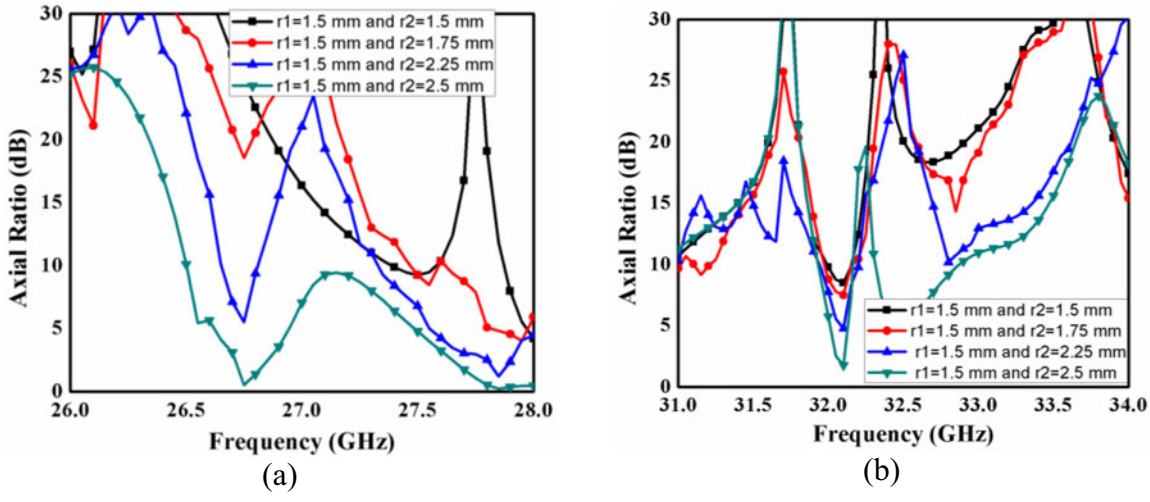

Figure 7. Axial ratio variation with variation in size of fan blade: (a) lower operating band and (b) upper operating band.

https://doi.org/10.1017/S1759078724000163 Published online by Cambridge University Press

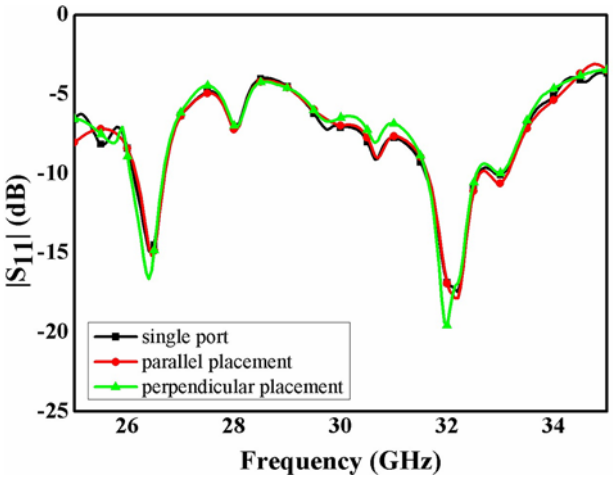

Figure 8. $|S_{11}|$ variation of single-port and dual-port (parallel and perpendicular placement) antennas.

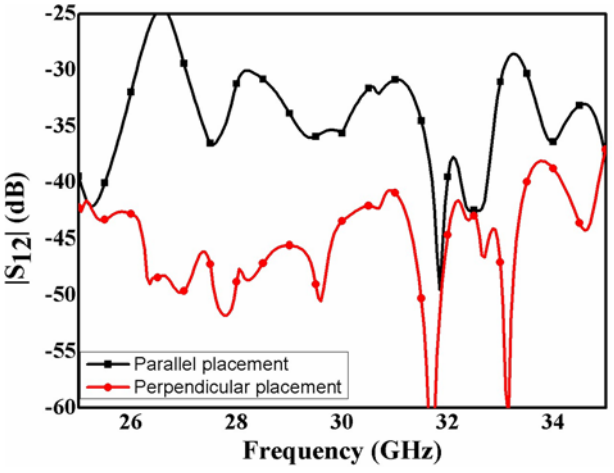

Figure 9. $|S_{12}|$ variation of parallel and perpendicular placement of dual-port antenna.

coupling reduced to −40 dB in case of perpendicular orientation. For this reason, perpendicular orientation has been chosen in the proposed one. Figure 10 shows the axial ratio variation with single-port and dual-port (with parallel and perpendicular orientation) antennas. It is confirmed that in all three cases, the axial ratio variation is approximately the same. It is required for MIMO antennas.

In the next step, a PRS is suspended over the radiator for tilts the radiation pattern obtained from different ports in different direction. In the proposed antenna, a superstrate that comprises of the parasitic square patches with continuous change in dimension, i.e. L_1, L_2, and L_3 is placed over the dual-port antenna. These patches are called as capacitive grids. Beam titling can be achieved by continuous phase variation. This can be done through constant change in dimension of parasitic square patches (Fig. 1(c)). Therefore, the proposed superstrate acts as the PRS [21]. Figure 11 shows the S-parameter variation in the absence and presence of PRS. From Fig. 11, it is confirmed that the S-parameter is approximately the

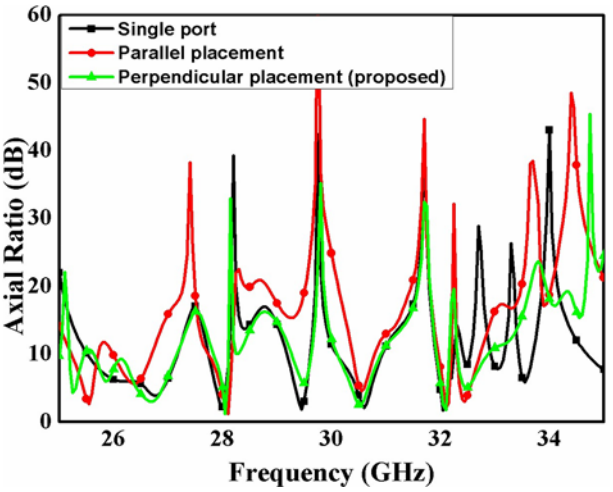

Figure 10. Axial ratio variation of single-port and dual-port (parallel and perpendicular placement) antennas.

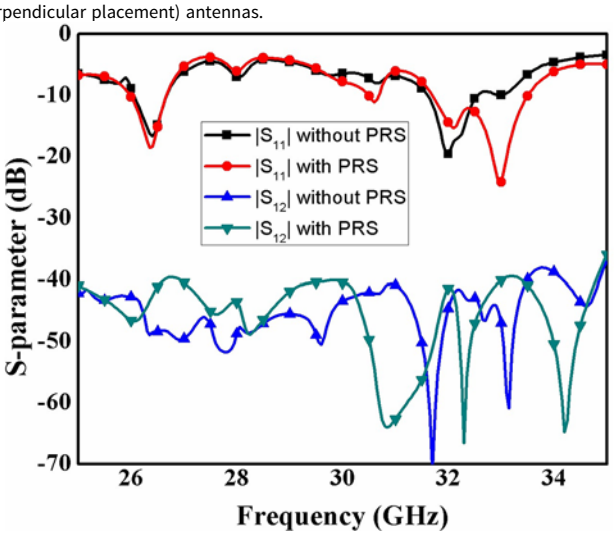

Figure 11. S-parameter variation of dual-port antenna in the presence/absence of PRS.

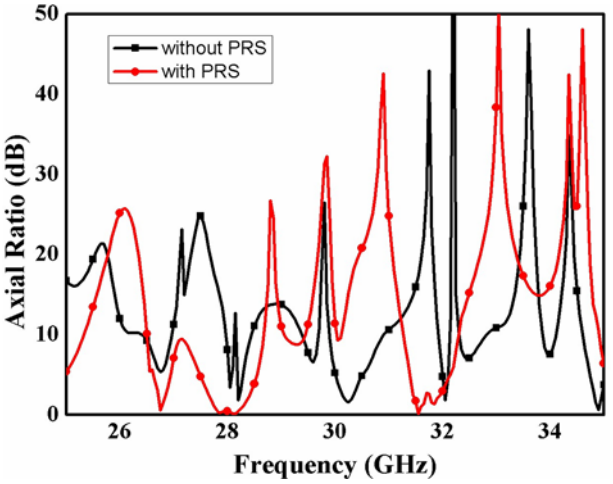

Figure 12. Axial ratio variation of dual-port antenna in the presence/absence of PRS.

https://doi.org/10.1017/S1759078724000163 Published online by Cambridge University Press

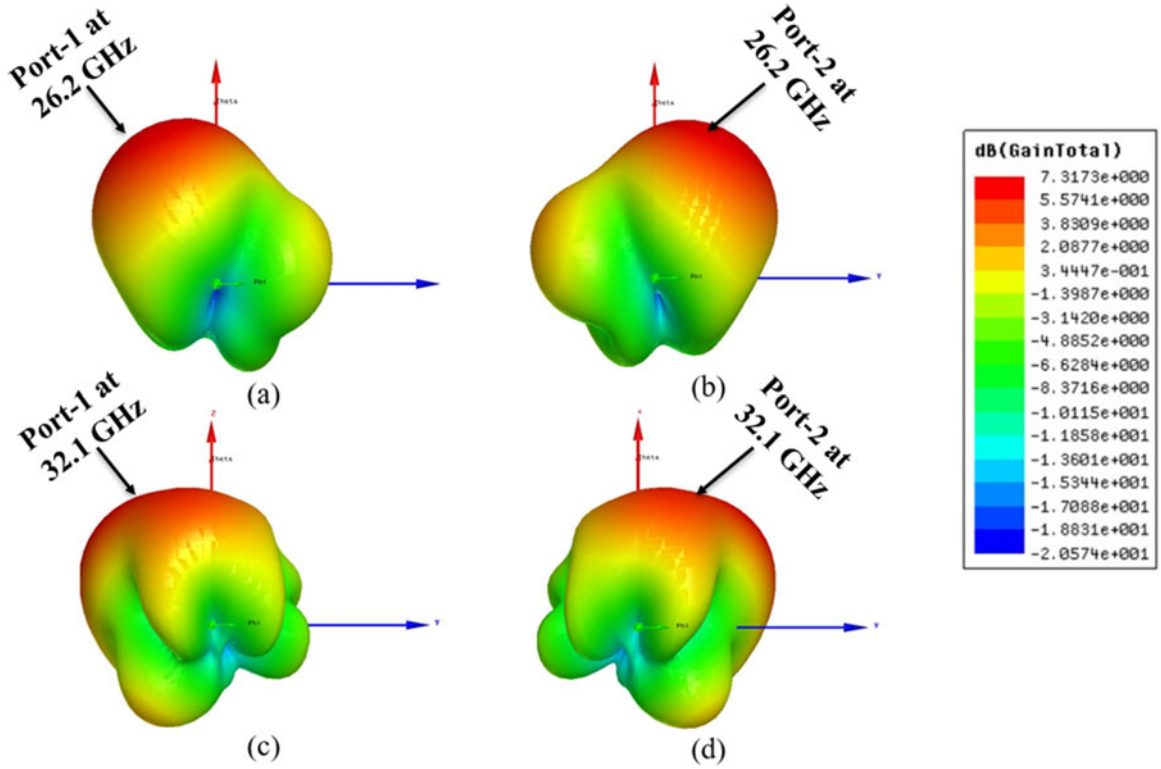

Figure 13. 3D polar plot of dual-port antenna with PRS: (a) Pprt-1 at 26.2 GHz, (b) port-2 at 26.2 GHz, (c) port-1 at 32.1 GHz, (d) port-2 at 32.1 GHz.

same in both the cases. Figure 12 shows the axial ratio plot in the absence and presence of PRS. From Fig. 12, there is minute change in the axial ratio in the absence and presence of PRS. Figure 13 shows the 3D radiation pattern in the presence of PRS with port-1 and port-2 at 26.2 GHz and 32.1 GHz, respectively. From Fig. 13, it can be perceived that the radiation pattern is tilted to −35° with port-1 at 26.2 GHz, while beam is tilted to +35° with port-2 at 26.2 GHz. Similarly, in upper frequency band (i.e. 32.1 GHz), the beam is tilted to −35° and +35° with port-1 and port-2, respectively. The 3D far-field pattern shown in Fig. 13 is obtained after placing the PRS. Therefore, it shows tilting from broadside direction. Without PRS, the radiation pattern is broadsided (i.e. follows the operating mode). In the designed PRS, the dimension of unit cell is changing from edge to middle. Due to this uneven distribution of unit cell, phase gradient has been changed. It will tilt the radiation beam in the opposite direction [22].

Experimental outcomes

In this section, experimentally measured antenna parameters are compared with optimized simulated results. Figure 14 shows the measured and simulated S-parameter for the proposed radiator. It is measured by using keysight-based E8363C PNA. From Fig. 14, it is observed that there is good agreement between measured and simulated S-parameter. The proposed antenna works in between dual frequency range (i.e. 26.1–27.5 GHz and 31.7–33.6 GHz, respectively). Isolation level is more than 35 dB between the ports. Figure 15(a) and (b) shows the measured and simulated axial ratio variation in lower and upper working frequency band, respectively. It is measured inside the anechoic chamber. From Fig. 15, it can be said that there is good agreement between measured and simulated axial ratio. The designed radiator supports the CP waves from

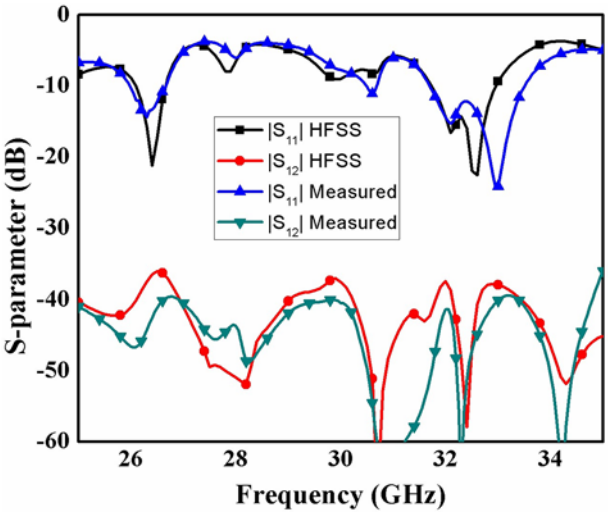

Figure 14. Measured and simulated S-parameter of the proposed radiator.

26.5 to 27.1 GHz and 31.9 to 33.1 GHz in lower and upper working frequency band, respectively. Figure 16 shows the measured and simulated 2D left- and right-handed circular polarization (RHCP) radiation patterns in XZ plane at 26.75 GHz and 31.5 GHz with port-1 and port-2, respectively. From Fig. 16, it is observed that the patterns obtained from port-1 and port-2 have been tilted in different direction by ±35°. Another observation obtained from Fig. 16 was that the designed radiator acts as RHCP with both the antenna ports. After seeing the radiation pattern, it can be observed that cross-pol level is high in the designed radiator. It is due to presence

https://doi.org/10.1017/S1759078724000163 Published online by Cambridge University Press

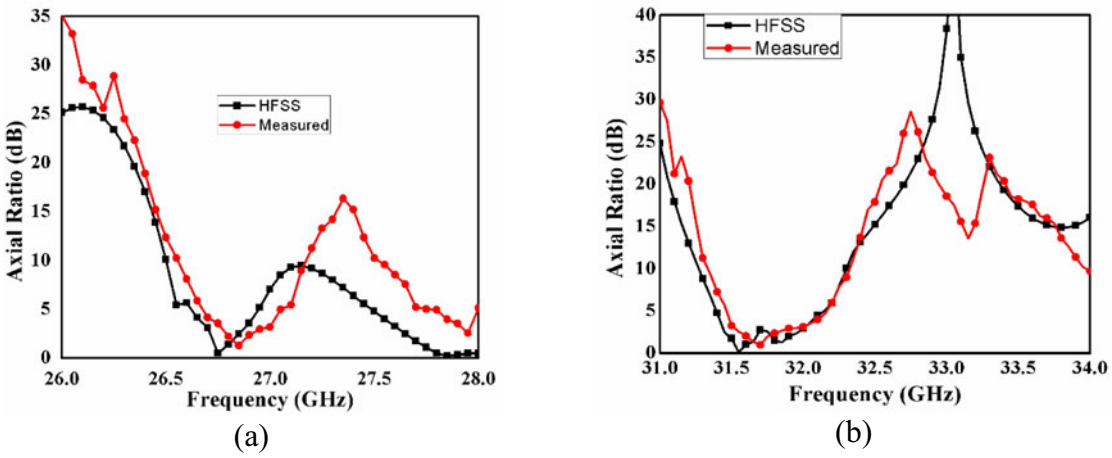

Figure 15. Measured and simulated axial ratio variation of the proposed antenna: (a) lower frequency band and (b) upper frequency band.

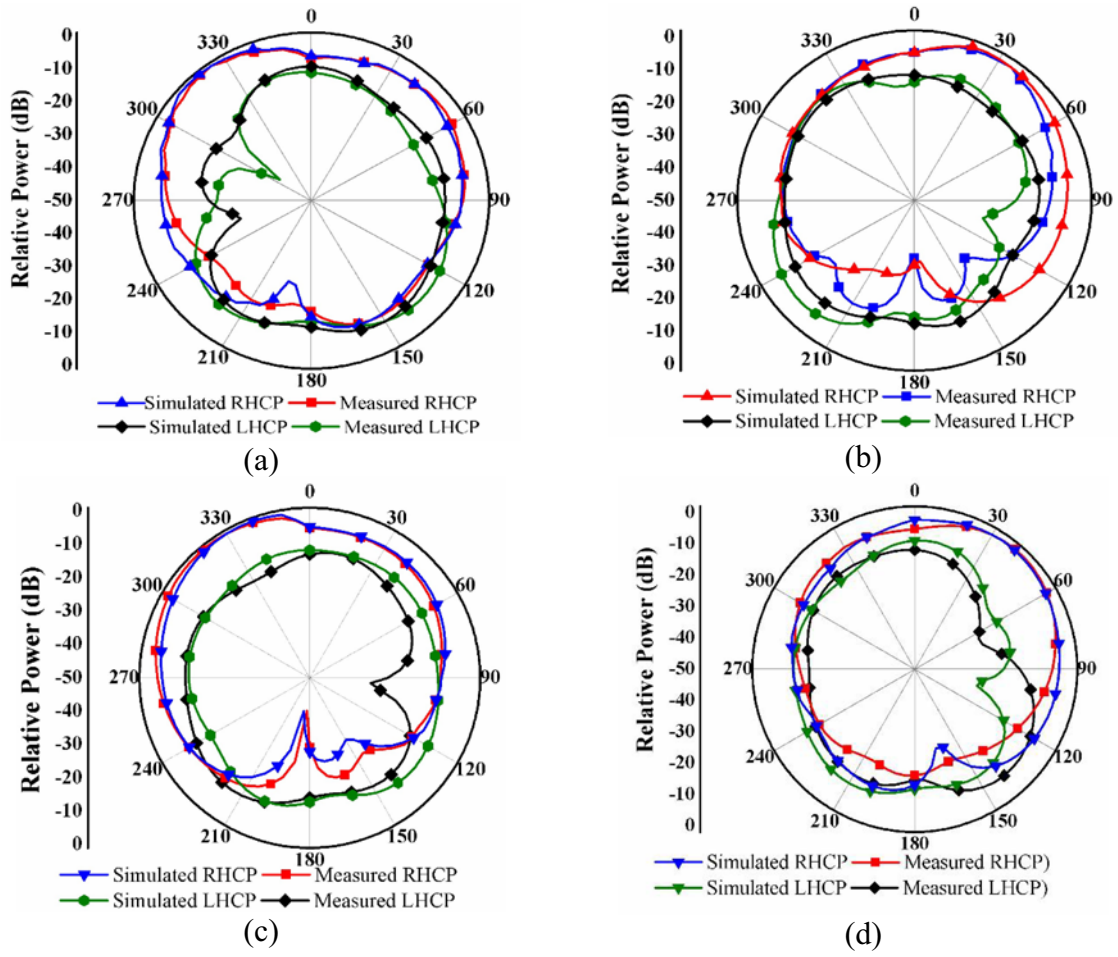

Figure 16. Measured and simulated LHCP and RHCP radiation pattern: (a) port-1 at 26.75 GHz, (b) port-2 at 26.75 GHz, (c) port-1 at 31.5 GHz, (d) port-2 at 31.5 GHz.

of PRS. In the presence of PRS, cross-pol level increases with increment in beam tilting. In the designed antenna, the cross-pol level is approximately 15 dB down in the direction of maximum radiation. It is a good value of efficient radiator. For the proposed radiator, the value of FBR is 5.7 dB and 6.4 dB at 26.1 GHz and 32.5 GHz. respectively. It is low because of the presence of aperture. One can improve the value of FBR by placing the reflector on the lower side of the substrate.

Figure 17 shows the gain and radiation efficiency variation of the designed radiator. Gain is calculated with the help of two antenna techniques [22]. From Fig. 17, it can be perceived that the radiation efficiency is more than 90% in the working band. The gain

https://doi.org/10.1017/S1759078724000163 Published online by Cambridge University Press

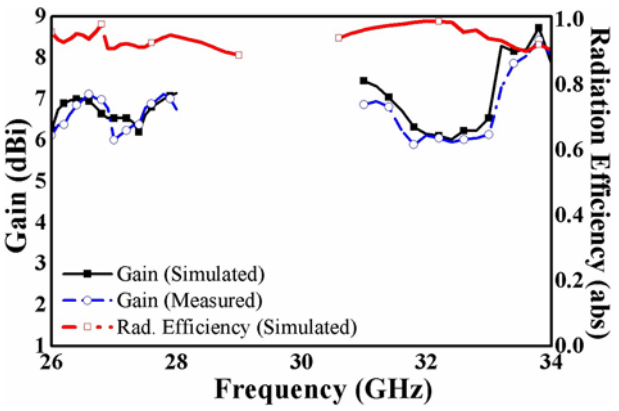

Figure 17. Gain (measured/simulated) and radiation efficiency (simulated) curve of the designed mm-wave antenna.

is approximately 7.0 dBi in both frequency ranges. Table 2 shows the performance comparison of the proposed dual-port ceramic-based mm-wave radiator with other existing antennas on the basis of impedance bandwidth, axial ratio bandwidth, gain, and pattern diversity. Data from Table 2 confirms the overall performance of the designed antenna is better in comparison to other existing ceramic-based mm-wave antenna.

Diversity factors such as envelop correlation coefficient (ECC) and diversity gain (DG) are highly significant in case of multi-port radiator. ECC tells about the correlation (either in terms of scattering or far-field parameter) between the ports [1]. For competent multi-port radiator, the ECC should be as low as possible. DG expresses the gain of diversity aerial in the fading situation [1]. Generally, the value of ECC of an efficient MIMO is taken as <0.3, while the DG is approximately 10 dB. There are two methods to measure the ECC and DG, i.e. by S-parameter and by far-field parameter. The following formulation is used for this purpose [1]:

$$^{*}\mathrm{ECC}_{\mathrm{S-parameter}} = \frac{\left|S_{11}^{*}S_{12} + S_{21}^{*}S_{22}\right|^{2}}{\left(\left(1-\left(|S_{11}|^{2}+|S_{21}|^{2}\right)\right)\left(1-\left(|S_{22}|^{2}+|S_{12}|^{2}\right)\right)\right)} \quad (3)$$

$$\mathrm{ECC_F} = \frac{\left|\iint_{4\pi}\left[E_i(\theta,\phi) * E_j(\theta,\phi)\right] \mathrm{d}\,\Omega\right|^{2}}{\iint_{4\pi}\left|E_i(\theta,\phi)\right|^{2}\mathrm{d}\,\Omega \iint_{4\pi}\left|E_j(\theta,\phi)\right|^{2}\mathrm{d}\,\Omega} \quad (4)$$

$$DG = \sqrt{1-ECC} \quad (5)$$

In eqn. (3–5), the symbols have their usual meaning. Figure 18 shows the DG and ECC variation of the designed aerial using S-parameter. From Fig. 18, it is perceived that the ECC is <0.15 and DG is around 10 dB inside the operating band. Table 3 provides the value of ECC and DG of the proposed antenna using far-field. From Table 3, the ECC and DG of the designed aerial are in the standard limit.

Conclusion

In this article, a two-port ceramic-based radiator at mm-wave frequency is structured and investigated. With the help of fan-shaped slot, the radiator works in dual frequency band, i.e. 26.1–27.5 GHz/31.7–33.6 GHz and also supports CP waves in both bands, i.e. 26.5–27.1 GHz/31.9–33.1 GHz. A PRS is suspended over

Table 2. Performance comparison of the designed antenna with other existing ceramic-based mm-wave antenna

Antenna structure	Impedance bandwidth (GHz)	Isolation (dB)	Axial ratio band-width	Gain (dBi)	Pattern diversity
Dual-port rectangular DRA [5]	1.34	>25	NA	8.0	NA
Dual-port rectangular DRA [6]	2.4	>35	NA	6.0	NA
Four-port rectangular DRA [7]	2.23	>25	NA	7.0	NA
Dual-port cylindrical DRA [8]	4.2	>35	NA	4.0	NA
Dual-port rectangular DRA [9]	4.5/3.15	>25	NA	8.0	NA
Dual-port cylindrical DRA [10]	2.29	>30	0.33	5.0	NA
Dual-port cylindrical DRA [11]	0.6	>25	NA	4.5	±45°
Dual-port semicylin-drical DRA [12]	2.1	>15	0.32	4.0	NA
Four-port Z-shaped DRA [13]	4.0	>20	0.8	6.0	NA
Dual-port epsilon DRA [14]	0.8	>15	NA	6.0	±35°
Rectangular DRA [15]	2.3	>20	NA	5.0	NA
Proposed antenna	1.6/1.9	>35	0.6/1.2	7.0	±35°

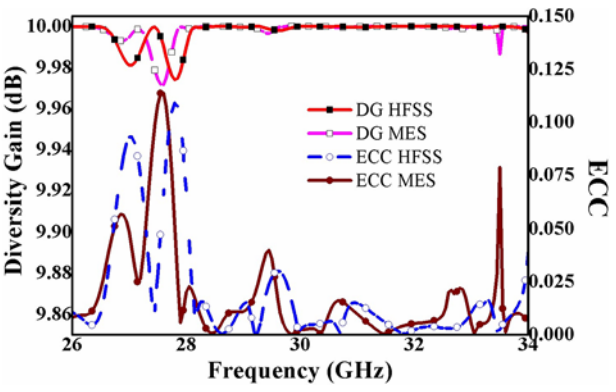

Figure 18. ECC and diversity gain curve of the designed mm-wave antenna.

https://doi.org/10.1017/S1759078724000163 Published online by Cambridge University Press

Table 3. Measured value of ECC and DG using far-field

Frequency (GHz)	ECC	DG	Frequency (GHz)	ECC	DG
26.1	0.154	9.751	31.7	0.168	9.701
26.5	0.149	9.769	32.1	0.154	9.751
26.9	0.116	9.795	32.5	0.137	9.802
27.1	0.099	9.845	33.1	0.112	9.815
27.5	0.126	9.804	33.6	0.125	9.803

the radiator for tilting the beam in opposite direction from different ports. It provides a beam tilt of $\pm 30^{\circ}$. Orthogonal placement of antenna ports provides the mutual coupling reduces to −35 dB in operating bands. All these appearances of the designed aerial find it appropriate for mm-wave 5G wireless communication system.

Funding statement. This research received no specific grant from any funding agency, commercial or not-for-profit sectors.

Competing interests. The authors report no conflict of interest.

References

1. **Sharawi MS** (2014) *Printed MIMO Antenna Engineering*. Boston: Artech House.
2. **Hong W** (2017) Solving the 5G mobile antenna puzzle: Assessing future directions for the 5G mobile antenna paradigm shift. *IEEE Microwave Magazine* **18**(7), 86–102.
3. **Kornprobst J, Wang K, Hamberger G and Eibert TF** (2017) A mm-wave patch antenna with broad bandwidth and a wide angular range. *IEEE Transactions on Antennas and Propagation* **65**(8), 4293–4298.
4. **Petosa A** (2007) *Dielectric Resonator Antenna Handbook*. Norwood, MA: Artech House.
5. **Zhang Y, Deng J-Y, Li M-J, Sun D and Guo L-X** (2019) A MIMO dielectric resonator antenna with improved isolation for 5G mm-wave applications. *IEEE Antennas and Wireless Propagation Letters* **18**, 747–751.
6. **Mei Pan Y, Qin X, Sun YX and Zheng SY** (2019) A simple decoupling method for 5G millimeter-wave MIMO dielectric resonator antennas. *IEEE Transactions on Antennas and Propagation* **67**(4), 2224–2234.
7. **Murthy NS** (2020) Improved isolation metamaterial inspired mm-wave MIMO dielectric resonator antenna for 5G application. *Progress in Electromagnetics Research C* **100**, 247–261.
8. **Hasan ML, Mabrouk IB, Almajali ERF, Nedil M and Denidni TA** (2019) Hybrid isolator for mutual-coupling reduction in millimeter-wave MIMO antenna systems. *IEEE Access* **7**, 58466–58474.
9. **Alanazi MD and Khamas SK** (2022) A compact dual band MIMO dielectric resonator antenna with improved performance for mm-wave applications. *Sensors* **22**, 5056.
10. **Kumar A, Dwivedi AK, Nagesh KN, Sharma A and Ranjan P** (2022) Circularly polarized dielectric resonator based two port filtenna for millimeter-wave 5G communication system. *IETE Technical Review* **39**, 1501–1511.
11. **Sharma D, Katiyar R, Dwivedi AK, Nagesh KN, Sharma A and Ranjan P** (2022) Dielectric resonator-based two-port filtennas with pattern and space diversity for 5G IoT applications. *International Journal of Microwave and Wireless Technologies* **15**, 263–270.
12. **Varshney G, Singh R, Pandey VS and Yaduvanshi RS** (2020) Circularly polarized two-port MIMO dielectric resonator antenna. *Progress in Electromagnetics Research M* **91**, 19–28.
13. **Ibrahim AA, Zahra H, Abbas SM, Ahmed MI, Varshney G, Mukhopadhyay S and Mahmoud A** (2022) Compact four-port circularly polarized MIMO X-band DRA. *Sensors* **22**(12), 4461.
14. **Varshney G, Gotra S, Chaturvedi S, Pandey VS and Yaduvanshi RS** (2019) Compact four-port MIMO dielectric resonator antenna with pattern diversity. *IET Microwaves, Antennas & Propagation* **13**(12), 2193–2198.
15. **Varshney G, Yaduvanshi RS, Ibrahim AA and Abdelhady MA** (2022) Technique of controlling the bandwidth of MIMO rectangular dielectric resonator antenna. *MAPAN - Journal of Metrology Society of India* **37**(2), 357–365.
16. **Kajfez D, Glisson AW and James J** (1984) Computed modal field distributions for isolated dielectric resonators. *IEEE Transactions on Microwave Theory & Techniques* **32**, 1609–1616.
17. **Mongia RK and Bhartia P** (1994) Dielectric resonator antennas-a review and general design relations for resonant frequency and bandwidth. *International Journal of Microwave and Millimeter-Wave Computer-Aided Engineering* **4**, 230–247.
18. **Sharma A, Das G, Gupta S and Gangwar RK** (2020) Quad-band quad-sense circularly polarized dielectric resonator antenna for GPS/CNSS/WLAN/WiMAX applications. *IEEE Antennas and Wireless Propagation Letters* **19**, 403–407.
19. **Guha D, Gupta P and Kumar C** (2015) Dual band cylindrical dielectric resonator antenna employing $HE_{11\delta}$ and $HE_{12\delta}$ mode excited by new composite structure. *IEEE Transaction on Antennas and Propagation* **63**(1), 433–438.
20. **Balanis CA** (2005) *Antenna Theory: Analysis and Design*, 3rd edn. New York: A John Wiley & Sons, INC., Publication.
21. **Qin F, Gao S, Mao C, Wei G, Xu J and Li J** (2015) Low-profile high gain tilted-beam Fabry-Perot antenna. In *2015 9th European Conference on Antennas and Propagation (EuCAP)*, 1–5
22. **Yu N, Genevet P, Kats MA, Aieta F, Tetienne JP, Capasso F and Gaburro Z** (2011) Light propagation with phase discontinuities: Generalized laws of reflection and refraction. *Science (80)* **334**(6054), 333–337.

Pawan Kumar Shukla born in Jaunpur, Uttar Pradesh, India, in 1989. He is a Research Scholar in the Electronics and Communication Engineering Department at Motilal Nehru National Institute of Technology Allahabad, Uttar Pradesh, India. He is completed his master's degree (M.Tech.) in Electronics and Communication Engineering from University of Allahabad, India, in 2020 and bachelor's degree in Electronics and Telecommunication Engineering from AMIETE New Delhi, India, in 2015. His research interests include DRA-based antenna design for mm-wave 5G application, metamaterial and metasurface physics, IoT.

Sikandar born in Ambedkar Nagar, Uttar Pradesh, India, in 1987. He is Assistant Professor in REC Sonbhadra, Uttar Pradesh, India. He received his B.Tech and M.Tech degrees from University of Allahabad, India, in 2010 and 2015, respectively. He has authored or co-authored for more than 10 research paper in international/national journal/conference proceedings. His area of interest is microwave antennas.

https://doi.org/10.1017/S1759078724000163 Published online by Cambridge University Press

Vijay Shanker Tripathi born in Gorakhpur, Uttar Pradesh, India, in 1965. He has completed his Ph.D. from Electronics and Communication Engineering department from Motilal Nehru National Institute of Technology Allahabad in 2007, M.E. in digital systems from Motilal Nehru National Institute of Technology in 1999 and B.Tech. in electronics and telecommunication engineering from University of Allahabad in 1988. Currently, he is Professor in department of electronics and communication engineering, Motilal Nehru National Institute of Technology Allahabad, Prayagraj, Uttar Pradesh, India. He has authored or coauthored over 70 research papers in international/national journal conference proceedings. His research interest includes RF circuits and systems, antenna, SDR, and noninvasive RF sensors.

Anand Sharma received his Bachelor of Technology from Uttar Pradesh Technical University Lucknow in 2012, Master of Technology from Jaypee University of Engineering and Technology Guna in 2014, and Ph.D. in RF and Microwave from Indian Institute of Technology (ISM), Dhanbad, in 2018. After that, he joined Government Engineering College Sonbhadra, Uttar Pradesh, as Assistant Professor in Electronics Engineering Department and left the college in June 2019. Currently, he holds the position of Assistant Professor in the Department of Electronics and Communication Engineering, Motilal Nehru National Institute of Technology Allahabad, Prayagraj, Uttar Pradesh, India. He has published more than 60 articles in the International Journal (SCI Indexed) and also presented more than 40 articles in National/International Conferences. His area of research includes MIMO antennas, antenna for IoT applications, circularly polarized DRAs, ultra-wideband and super wideband antennas, wearable antennas, and antenna optimization using machine learning.

https://doi.org/10.1017/S1759078724000163 Published online by Cambridge University Press